Evanescent-wave coupled right angled buried waveguide: Applications in carbon nanotube mode-locking

R. Mary,[1] G. Brown,[2] S. J. Beecher,[3] R. R. Thomson,[1] D. Popa,[4] Z. Sun,[4] F. Torrisi,[4] T. Hasan,[4] S. Milana,[4] F. Bonaccorso,[4] A. C. Ferrari,[4] and A. K. Kar[1,a)]
[1]*Institute of Photonics and Quantum Sciences, Heriot-Watt University, Edinburgh EH14 4AS, United Kingdom*
[2]*Optoscribe Ltd, 0/14 Alba Innovation Centre, Alba Campus, Livingston EH54 7GA, United Kingdom*
[3]*Optoelectronics Research Centre, University of Southampton, Southampton SO17 1BJ, United Kingdom*
[4]*Cambridge Graphene Centre, University of Cambridge, Cambridge CB3 0FA, United Kingdom*

(Received 24 September 2013; accepted 13 November 2013; published online 27 November 2013)

We present an evanescent-field device based on a right-angled waveguide. This consists of orthogonal waveguides, with their points of intersection lying along an angled facet of the chip. Light guided along one waveguide is incident at the angled dielectric-air facet at an angle exceeding the critical angle, so that the totally internally reflected light is coupled into the second waveguide. By depositing a nanotube film on the angled surface, the chip is then used to mode-lock an Erbium doped fiber ring laser with a repetition rate of 26 MHz, and pulse duration of 800 fs. © *2013 AIP Publishing LLC*. [http://dx.doi.org/10.1063/1.4834360]

Evanescent field generation by total internal reflection (TIR) finds numerous applications in sensors,[1–4] evanescent-wave spectroscopy,[5–7] and optoelectronics.[8] When light travelling from a denser to a rarer medium strikes the boundary at an angle greater than the critical angle, the wave is entirely reflected while generating an exponentially decaying evanescent field in the lower index medium.[9] With the capability to overcome the diffraction limit, evanescent wave interaction has become the key principle for various sensing technologies, including infrared spectroscopy,[5,6] TIR fluorescence microscopy[4,7] and surface plasmon resonance (SPR) sensors.[1,2,4] SPR sensors work by the principle of frustrated TIR,[9] where the evanescent wave is coupled to a denser third medium placed very close to the interface of the evanescent field generator, at the expense of reflectivity at the first interface.[9] With the rapid advances in lasers and fiber optics, evanescent wave sensing has been ever-evolving: fast,[2,6] automated[6] devices based on optical fibers and photonic circuit technology have already been developed.[2,4,6] In optical fibers, the evanescent field in the core-cladding interface has been exploited for various sensing applications by using different geometries, such as de-cladded,[4] tapered,[2,4,6] U-shaped[2,6] and tapered tip optical fibers.[4] The sensors work by monitoring perturbations in the exponentially decaying field in the presence of an external medium, with the fiber acting as a modulator. In comparison to conventional bulk sensing elements, fiber optic technology offers enhanced sensitivity, versatility in configuration geometry, and device miniaturisation, with the reflected light at the interface guided down the fiber. This technique also allows distributed sensing[2,4,6] and multiplexing capabilities,[6] while being less sensitive to scattering and variations in the excitation signal.[2,4,6]

Carbon nanotubes (CNTs) and graphene have emerged as excellent passive mode-lockers because of their sub-picosecond recovery time,[10–12] broad operation range,[13,14] low saturation intensity,[15,16] low cost,[15] and ease of fabrication.[13,14,16–23] A variety of techniques have been implemented in order to integrate these novel saturable absorbers (SAs) into lasers.[18] Evanescent field interaction[24,25] can preserve the alignment-free waveguide format of a variety of laser designs,[18] e.g., waveguide[26] and semiconductor,[27] for high power/energy pulse generation. This technology can also enable compact lasers with GHz repetition rates.[28] CNTs and graphene SAs for evanescent field interaction have either been sprayed[23,24] or embedded into polymer matrices.[29,30] Evanescent field passive mode-locked fiber lasers have been designed based on various lateral interaction schemes, to couple light with CNTs[18,25] or graphene SAs.[18,24] In the side-polished fiber format,[24,25,30] a section of fiber cladding is removed to make a D-shaped fiber, reducing the distance between the external material and the guided mode.[23,24,28] The evanescent field of the mode then interacts with the SA to induce a modulation in the laser cavity.[23,24,28] Polymer composites can be easily integrated into a range of photonic systems.[15,18,31] When in resonance with the laser operating wavelength, CNT composites exhibit large (e.g., up to ~17% (Ref. 16)) modulation depth, typically needed in fiber lasers to ensure self-starting and operation stability.[32] Other methods of evanescent field interaction include the use of tapered fibers,[29] and accurately placed micromachined slots within fibers to allow for optimal mode interaction with the SA.[33] These lateral schemes allow longer interaction lengths,[29] while preserving the compact, alignment-free, laser configurations. However, they require micron scale precision[33] and, in the case of tapered fibers, *in-situ* monitoring to allow efficient mode-locking.[29]

With the advances in microfabrication technologies, evanescent field sensing has been extended to planar waveguide circuits.[3,8] Single chip sub-wavelength structures based on evanescent field interaction have the same advantages of optical fiber technology, while providing scope for further miniaturisation. Also, the feasibility of batch production provides the advantage of lowering cost. A simple and flexible method for microfabrication utilizes pulses of few hundred femtoseconds duration focussed beneath the substrate surface to create a refractive index change at the focus, by virtue of

a)Electronic mail: a.k.kar@hw.ac.uk

nonlinear absorption processes.[34] Translation of the sample along a desired trajectory extends this modification and can be used to fabricate waveguides. This technique of ultrafast laser inscription (ULI)[34] offers 3-dimensional fabrication capabilities with low insertion losses.

Here, we demonstrate a ULI based single chip device with efficient evanescent field coupling. The design of the device allows light in one waveguide to be totally internally reflected at the angled dielectric-air interface and coupled into another orthogonal waveguide. We prove the potential of this device for evanescent field interaction mode-locking of an Erbium-doped fiber ring laser. We use CNTs embedded into a polymer composite as SA, which can be uniformly deposited on the waveguide facet.[15] Mode-locked pulses at a repetition rate of 26 MHz, and with 800 fs pulse duration are generated by the interaction of the evanescent field with the CNT-SA deposited at the angled facet of the right angled buried waveguide.

A $30 \times 10 \times 1\,\text{mm}^3$ glass (Corning EAGLE 2000) is used as the substrate for the waveguide device. Waveguides are inscribed using a master-oscillator power-amplifier fiber laser (IMRA FCPA μ-Jewel D400) set to a repetition rate of 500 kHz, producing ~400 fs pulses centred at 1047 nm. A 0.4 numerical aperture (NA) aspheric lens is used to focus the pulse train to a depth of 350 μm. Waveguides are inscribed by translating the sample through the focus in the desired trajectory, using high precision automated x-y-z translation stages (Aerotech). A multiscan technique,[35] with 20 scans laterally offset by 0.4 μm, is used to define the waveguide cross-section. The optimal parameters for waveguide inscription are 230 nJ laser pulse energy at $8.0\,\text{mm.s}^{-1}$ sample translation speed.

The device design consists of 50 orthogonal waveguides inscribed with a 100 μm vertical pitch, and a slightly offset 102.8 μm horizontal pitch, as given in Fig. 1(a). The points of intersection of these waveguides therefore lie at an angle of 45.8°. Post-inscription, the substrate is diced at 45°, and polished along the dice line. The ~0.8° difference in angles between the dice line and the line formed by the intersection points of the waveguides is chosen so that there is always one waveguide vertex within 1 μm of the polished facet, allowing efficient waveguide-waveguide coupling by TIR. The facets that constitute the start and termination of the orthogonal waveguide geometry are also ground and polished to avoid detrimental perforation effects of the inscription beam.[36] Passive characterization of the device using a broadband amplified spontaneous emission (ASE) source, and butt-coupled single mode fibers (SMF-28) yield an insertion loss of less than 1 dB (i.e., 1.26 input/output power ratio).

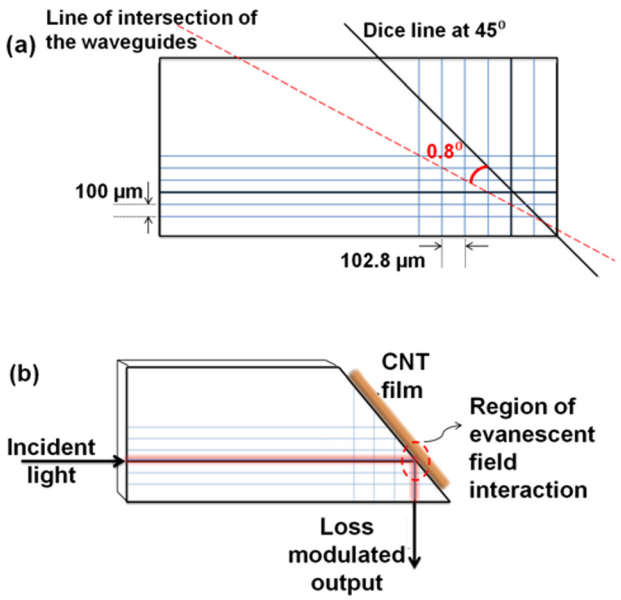

FIG. 1. (a) Waveguide layout and dicing location. (b) The principle of evanescent field coupling at the angled facet of the waveguide device.

For SA deposition on the waveguide facet, a polymer dispersion allows rapid formation of a uniform composite upon evaporation of water,[15] resulting in a low-cost, room-temperature fabrication process, in the meantime acting as a protective layer for the waveguide facet.[15] A graphene-composite can operate as a full-bandwidth SA.[31] However graphene-embedded polymers exhibit low (e.g., ~1%–2% (Refs. 20 and 21)) modulation depths. A broad operation range can also be achieved in CNTs, by using a diameter distribution.[13] When in resonance with the laser operating wavelength, CNTs can offer high (i.e., up to ~17% (Ref. 16)) modulation depth, which is typically needed in fiber lasers.[32] Thus, we use a CNT-composite SA, which can be easily drop-cast on our waveguide facet fiber-based laser. Sodium carboxymethylcellulose (Na-CMC) can be used both as dispersant and host polymer matrix, allowing fabrication of composites with no need of surfactants (e.g., sodium dodecyl sulfate),[37] and eliminating the additional step of introducing a host polymer (such as polyvinyl alcohol)[15] in the dispersion before the solvent is evaporated.[15]

For the laser operating wavelength, ~1.5 μm, we need tubes with ~1.3 nm diameter.[38] For this, we use laser ablation (LA) single wall nanotubes (SWNTs),[39] with a broad band centred at ~1.5 μm in the absorbance spectrum shown in Fig. 2(a). This band corresponds to the first excitonic transition (eh_{11})[40] of SWNTs with diameter ranging from ~1.15 nm [e.g., (14,1), (13,3)], ~1.25 nm [e.g., (11,7)] to ~1.3–1.38 nm [e.g., (12,7), (16,2), (15,4)], as confirmed from the corresponding peaks [e.g., (14,1) at ~750 nm, (13,3) at ~765 nm, (11,7) at ~835 nm, (12,7) at ~930 nm, and (16,2) and (15,4) at ~985nm], in the 750–1050 nm range, associated to the second excitonic transition (eh_{22}).[40] To further investigate the tube diameter distribution, before and after composite fabrication, and monitor defects, we measure the Raman spectra of the starting powder and the composite at 457, 514.5, and 633 nm excitation. In the low frequency region, the Radial Breathing Modes (RBMs) are observed.[41] Their position [Pos(RBM)] is inversely related to CNT diameter, d_t[42–44] by the relation $\text{Pos(RBM)} = \frac{C_1}{d_t} + C_2$. Combining Pos(RBM) with excitation wavelength and the "Kataura plot,"[45] it is, in principle, possible to derive the SWNT chirality. Matching the diameter given by Pos(RBM) with the excitation wavelength in the Kataura plot also gives information on the semiconducting (s-) or metallic (m-) character. A variety of C_1 and C_2 were proposed, see e.g., Refs. 41–43, 46. Here we use $C_1 = 214.4\,\text{cm}^{-1}$ nm and $C_2 = 18.7\,\text{cm}^{-1}$, derived in Ref. 44 by plotting the resonance energy as a function of Pos(RBM)^{-1} without any additional assumptions. The

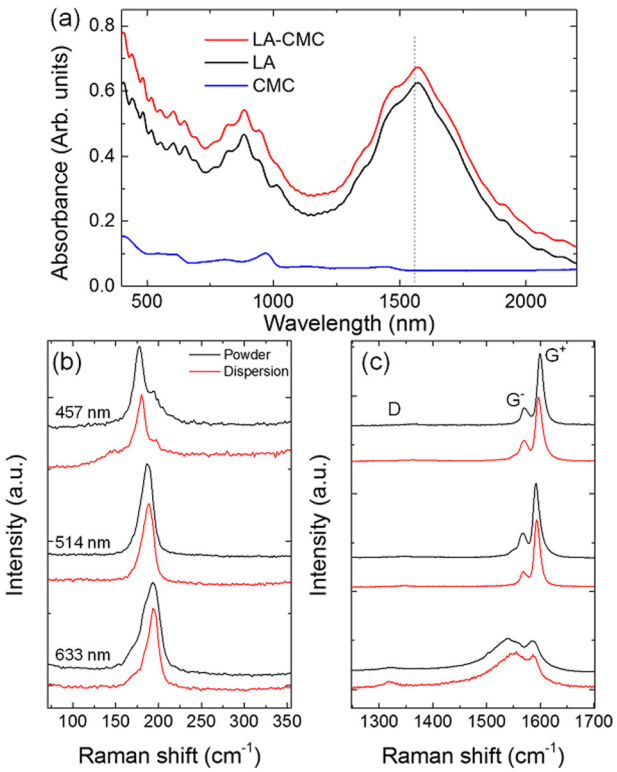

FIG. 2. (a) Absorbance of LA-SWNTs and CMC. Our mode-locked laser operating wavelength is marked. Raman spectra measured at 457, 514, and 633 nm for (black lines) LA-SWNT powders and (red line) LA-SWNTs dispersed in CMC in the (b) RBM and (c) G peak region.

typical Raman spectrum of SWNTs in the 1500–1600 cm^{-1} range is dominated by the G^+ and G^- bands.[47,48] In s-SWNTs, they originate from the longitudinal (LO) and tangential (TO) modes, respectively, derived from the splitting of the E_{2g} phonon of graphene.[49–51] Pos(G^+) and Pos(G^-) are diameter dependent,[49] and the separation between them increases with decreasing diameter. Thus, Pos(G^+) and Pos(G^-) can be used to determine the diameter distribution.[49,52] In m-SWNTs, the G^+, G^- assignment is the opposite, the Full Width Half Maximum of the G peak [FWHM(G^-)] is larger, and Pos(G^-) down-shifted with respect to s-SWNTs.[49,50] From the analysis of RBMs,[42] G peak,[49] and FWHMs,[49] we estimate the diameter to be in the 1.2–1.4 nm range, in agreement with optical absorption.

The CNT-SA is then prepared as follows. ~0.03 wt.% LA-SWNTs powder is ultrasonicated in deionized water with CMC for 1 h. The resultant dispersion is then ultracentrifuged for 2 h at 35 000 rpm to remove insoluble particles and CNT aggregates, and the supernatant collected.[53] The absorption of the CNT-CMC composite [Red line Fig. 2(a)] shows the same features of the starting material (black line), thus the presence of CMC does not affect the optical properties of CNTs. The CNT composite is deposited on the angle facet of the waveguide by drop-casting and dried over 24 h. The Raman spectrum of the deposited composite is shown in Figs. 2(b) and 2(c) (red lines). For all excitation wavelengths we do not observe any change in the distribution of Pos(RBM), Pos(G^+), Pos(G^-), and FWHM(G^+) with respect to the starting powder (black lines). There is no change in the D peak position, width and intensity, indicating that the dispersion process[53] and the polymer-composite fabrication do not induce additional defects[47] with respect to the starting material.

The saturable absorption of the CNT film at 1550 nm is measured using an optical parametric oscillator (Coherent, Chameleon) delivering 200 fs pulses at 80 MHz repetition rate.[16] The CNT film has a linear transmittance of 33%, with saturation at 50%. This results in a modulation depth of 17%. The saturation intensity is 12.4 MW/cm^2.

The CNT-SA coated waveguide device is then integrated in an Er-based fiber ring cavity with 1 dB insertion loss, as shown in Fig. 3. The 980 nm pump laser is introduced into the ring cavity using a fiber based wavelength division multiplexer (WDM). A fiber optic isolator ensures unidirectional operation, and a polarization controller matches the round-trip polarization state. A broadband fused fiber 80:20 coupler (JDS Uniphase) is used to extract the laser output. The gain section of fiber laser consists of a 46.8 cm Liekki Er80-8/125 Erbium-doped fiber with an anomalous dispersion of $-20\ fs^2/mm$. The CNT-SA-waveguide device with fibers butt-coupled to orthogonal waveguide facets completes the ring cavity. An index matching fluid is used to reduce reflections between fiber and substrate facets. The remaining cavity length comprises 533.8 cm Corning SMF-28, 35.4 cm Corning Flexcore 1060, and 155.4 cm OFS Clearlight 980 16 fibers; with their corresponding linear dispersion values estimated as 17.9 ps/nm.km, 8 ps/nm.km, and −1 ps/nm.km. Assuming the dispersion contribution from the waveguide chip to be negligible, the measured net dispersion in the cavity is anomalous, with a value of $-0.13\ ps^2$, thereby enabling soliton mode-locking.

Self-starting mode-locking is obtained as a result of evanescent field interaction with the CNT-SA at the right angled waveguide geometry (Fig. 1(b)), producing a 1.3 mW average output power. This corresponds to 50 pJ pulse energy, considering the 26 MHz repetition rate of the mode-locked pulses determined with an RF spectrum analyser. The optical spectrum measured using an Optical Spectrum Analyser set to 0.05 nm resolution is given in Fig. 4. The spectrum of the mode-locked laser is centred at 1558 nm, with a FWHM spectral width of 3 nm. It shows Kelly

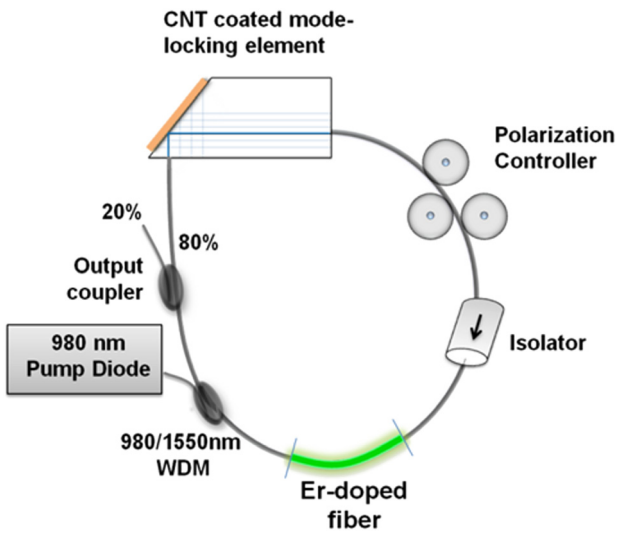

FIG. 3. Schematic of the mode-locked laser.

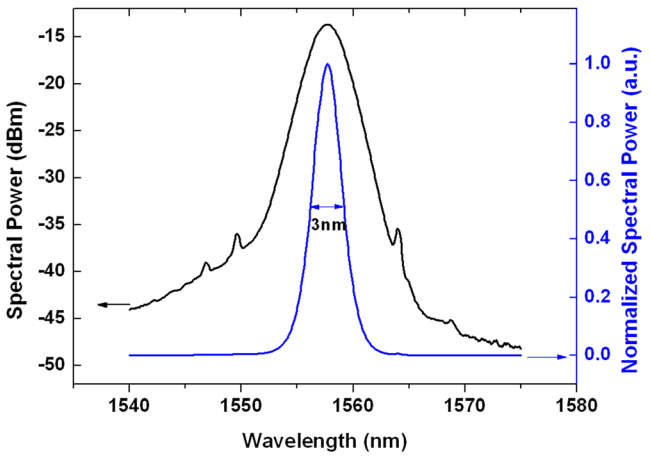

FIG. 4. Optical Spectra of the output from the laser in (black line) logarithmic scale and (blue line) linear scale.

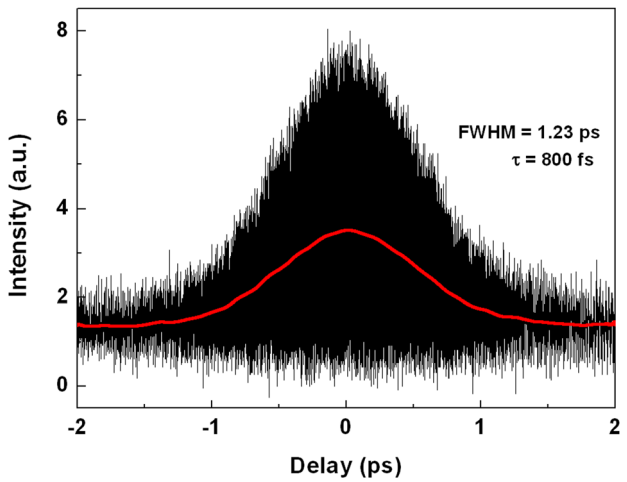

FIG. 5. Interferometric autocorrelation trace of the mode-locked laser.

sidebands,[54] i.e., narrow peaks superimposed to the optical spectrum related to a periodic disturbance of soliton pulses in the cavity.[54] The autocorrelation pulse profile derived from an interferometric autocorrelator is given in Fig. 5. The FWHM pulse width is estimated to be 800 fs, assuming a $sech^2$ pulse shape. This yields a time-bandwidth product (TBP) of 0.30, close to 0.315, expected for bandwidth-limited $sech^2$-shaped pulses.[55]

As an evanescent-field mode-locker, our right-angle waveguide device has a number of advantages over previous fiber-based designs, e.g., in side-polished and fiber tapered devices, in order to expose a region close enough to the fiber core so as to achieve sufficient non-linear absorption, the polishing and fiber-pulling processes have to be extremely precise,[56] and carefully monitored.[56] Also, the exposed region has to be of sufficient length (~6 mm[29]) to overcome the considerably lower evanescent field penetration in the parallel configuration.[57] Our integrated waveguide device has no need for precision polishing, nor critical optical monitoring by virtue of the variation in the horizontal and vertical waveguide pitches. In addition, the right-angle design ensures an increased penetration depth of the evanescent-field into the CNT-SA, corresponding to a nonlinear absorption interaction length of the order of the waveguide mode diameter. This, in turn, reduces the required deposition surface area. Even though our waveguide-based ring-cavity laser strays from the increased alignment-free format characteristic of fiber systems, it is an excellent demonstration of the scope of the waveguide device. This design can be applied to gain media to develop monolithic waveguide laser sources, which find important applications in integrated optics. Also, the inherent simplicity of the waveguide design and the reduced footprint for evanescent field interaction have huge implications for sensing applications, especially for robust SPR sensors and lab-on-chip devices.

In conclusion, we presented a single chip evanescent field device based on a right angle waveguide with the ability to interrogate a small area of a surface at a pre-defined angle, with no need for free-space components. This is an ideal platform for robust surface plasmon resonance sensors. This geometry of interaction was achieved using buried waveguides with loss sufficiently low for the component to be placed intracavity to mode-lock a fiber laser.

We acknowledge funding from EPSRC Grant Nos. EP/G030480/1, EP/K01711X/1, EP/K017144/1, ERC Grant NANOPOTS, ERC Synergy grant Hetero2D, EU Graphene Flagship, a Royal Society Wolfson Research Merit Award, The Royal Academy of Engineering, Emmanuel College and King's College, Cambridge, a Newton International Fellowship and the Newton Trust Cambridge.

[1]L. Wu, H. S. Chu, W. S. Koh, and E. P. Li, Opt. Express **18**, 14395 (2010).
[2]B. D. Gupta and R. K. Verma, J. Sens. **2009**, 979761 (2009).
[3]K. Schmitt, K. Oehse, G. Sulz, and C. Hoffmann, Sensors **8**, 711 (2008).
[4]A. Leung, P. M. Shankar, and R. Mutharasan, Sens. Actuators B **125**, 688 (2007).
[5]A. C. Jones and M. B. Raschke, Nano Lett. **12**, 1475 (2012).
[6]Y. Raichlin and A. Katzir, Appl. Spectrosc. **62**, 55 (2008).
[7]D. Toomre and D. J. Manstein, Trends Cell Biol. **11**, 298 (2001).
[8]A. W. Fang, H. Park, Y.-h. Kuo, R. Jones, O. Cohen, D. Liang, O. Raday, M. N. Sysak, M. J. Paniccia, and J. E. Bowers, Mater. Today **10**, 28 (2007).
[9]A. W. Snyder and J. D. Love, *Optical Waveguide Theory* (Chapman and Hall, London, New York, 1983), p.viii.
[10]J. S. Lauret, C. Voisin, G. Cassabois, C. Delalande, P. Roussignol, O. Jost, and L. Capes, Phys. Rev. Lett. **90**, 057404 (2003).
[11]D. Brida, A. Tomadin, C. Manzoni, Y. J. Kim, A. Lombardo, S. Milana, R. R. Nair, K. S. Novoselov, A. C. Ferrari, G. Cerullo, and M. Polini, Nat. Commun. **4**, 1987 (2013).
[12]A. Tomadin, D. Brida, G. Cerullo, A. C. Ferrari, and M. Polini, Phys. Rev. B **88**, 035430 (2013).
[13]F. Wang, A. G. Rozhin, V. Scardaci, Z. Sun, F. Hennrich, I. H. White, W. I. Milne, and A. C. Ferrari, Nat. Nanotechnol. **3**, 738 (2008).
[14]Z. Sun, D. Popa, T. Hasan, F. Torrisi, F. Wang, E. Kelleher, J. Travers, V. Nicolosi, and A. Ferrari, Nano Res. **3**, 653 (2010).
[15]T. Hasan, Z. Sun, F. Wang, F. Bonaccorso, P. H. Tan, A. G. Rozhin, and A. C. Ferrari, Adv. Mater. **21**, 3874 (2009).
[16]D. Popa, Z. Sun, T. Hasan, W. B. Cho, F. Wang, F. Torrisi, and A. C. Ferrari, Appl. Phys. Lett. **101**, 153107 (2012).
[17]C. E. S. Castellani, E. J. R. Kelleher, D. Popa, T. Hasan, Z. Sun, A. C. Ferrari, S. V. Popov, and J. R. Taylor, Laser Phys. Lett. **10**, 015101 (2013).
[18]Z. Sun, T. Hasan, and A. C. Ferrari, Physica E (Amsterdam) **44**, 1082 (2012).
[19]M. Zhang, E. J. R. Kelleher, F. Torrisi, Z. Sun, T. Hasan, D. Popa, F. Wang, A. C. Ferrari, S. V. Popov, and J. R. Taylor, Opt. Express **20**, 25077 (2012).
[20]Z. Sun, T. Hasan, F. Torrisi, D. Popa, G. Privitera, F. Wang, F. Bonaccorso, D. M. Basko, and A. C. Ferrari, ACS Nano **4**, 803 (2010).
[21]D. Popa, Z. Sun, F. Torrisi, T. Hasan, F. Wang, and A. C. Ferrari, Appl. Phys. Lett. **97**, 203106 (2010).

[22]Z. Sun, A. G. Rozhin, F. Wang, T. Hasan, D. Popa, W. O'Neill, and A. C. Ferrari, Appl. Phys. Lett. **95**, 253102 (2009).
[23]V. Scardaci, Z. Sun, F. Wang, A. G. Rozhin, T. Hasan, F. Hennrich, I. H. White, W. I. Milne, and A. C. Ferrari, Adv. Mater. **20**, 4040 (2008).
[24]Y.-W. Song, S.-Y. Jang, W.-S. Han, and M.-K. Bae, Appl. Phys. Lett. **96**, 051122 (2010).
[25]Y.-W. Song, S. Yamashita, C. S. Goh, and S. Y. Set, Opt. Lett. **32**, 148 (2007).
[26]J. Clark and G. Lanzani, Nat. Photonics **4**, 438 (2010).
[27]U. Keller and A. C. Tropper, Phys. Rep. **429**, 67 (2006).
[28]R. Mary, G. Brown, S. J. Beecher, F. Torrisi, S. Milana, D. Popa, T. Hasan, Z. Sun, E. Lidorikis, S. Ohara, A. C. Ferrari, and A. K. Kar, Opt. Express **21**, 7943 (2013).
[29]Z. Q. Luo, J. Z. Wang, M. Zhou, H. Y. Xu, Z. P. Cai, and C. C. Ye, Laser Phys. Lett. **9**, 229 (2012).
[30]C. S. Jun, J. H. Im, S. H. Yoo, S. Y. Choi, F. Rotermund, D.-I. Yeom, and B. Y. Kim, Opt. Express **19**, 19775 (2011).
[31]F. Bonaccorso, Z. Sun, T. Hasan, and A. C. Ferrari, Nat. Photonics **4**, 611 (2010).
[32]O. Okhotnikov, *Fiber Lasers* (Wiley-VCH, Berlin, 2012).
[33]A. Martinez, K. Zhou, I. Bennion, and S. Yamashita, Opt. Express **18**, 11008 (2010).
[34]N. D. Psaila, R. R. Thomson, H. T. Bookey, A. K. Kar, N. Chiodo, R. Osellame, G. Cerullo, A. Jha, and S. Shen, Appl. Phys. Lett. **90**, 131102 (2007).
[35]R. Mary, S. J. Beecher, G. Brown, R. R. Thomson, D. Jaque, S. Ohara, and A. K. Kar, Opt. Lett. **37**, 1691 (2012).
[36]R. Osellame, G. Cerullo, and R. Ramponi, *Femtosecond Laser Micromachining* (Springer, 2012).
[37]N. Minami, Y. Kim, K. Miyashita, S. Kazaoui, and B. Nalini, Appl. Phys. Lett. **88**, 093123 (2006).
[38]R. B. Weisman and S. M. Bachilo, Nano Lett. **3**, 1235 (2003).
[39]S. Lebedkin, P. Schweiss, B. Renker, S. Malik, F. Hennrich, M. Neumaier, C. Stoermer, and M. M. Kappes, Carbon **40**, 417 (2002).
[40]M. J. O'Connell, S. M. Bachilo, C. B. Huffman, V. C. Moore, M. S. Strano, E. H. Haroz, K. L. Rialon, P. J. Boul, W. H. Noon, C. Kittrell, J. Ma, R. H. Hauge, R. B. Weisman, and R. E. Smalley, Science **297**, 593 (2002).
[41]A. M. Rao, E. Richter, S. Bandow, B. Chase, P. C. Eklund, K. A. Williams, S. Fang, K. R. Subbaswamy, M. Menon, A. Thess, R. E. Smalley, G. Dresselhaus, and M. S. Dresselhaus, Science **275**, 187 (1997).
[42]C. Fantini, A. Jorio, M. Souza, M. S. Strano, M. S. Dresselhaus, and M. A. Pimenta, Phys. Rev. Lett. **93**, 147406 (2004).
[43]J. C. Meyer, M. Paillet, T. Michel, A. Moréac, A. Neumann, G. S. Duesberg, S. Roth, and J.-L. Sauvajol, Phys. Rev. Lett. **95**, 217401 (2005).
[44]H. Telg, J. Maultzsch, S. Reich, F. Hennrich, and C. Thomsen, Phys. Rev. Lett. **93**, 177401 (2004).
[45]H. Kataura, Y. Kumazawa, Y. Maniwa, I. Umezu, S. Suzuki, Y. Ohtsuka, and Y. Achiba, Synth. Met. **103**, 2555 (1999).
[46]P. T. Araujo, S. K. Doorn, S. Kilina, S. Tretiak, E. Einarsson, S. Maruyama, H. Chacham, M. A. Pimenta, and A. Jorio, Phys. Rev. Lett. **98**, 067401 (2007).
[47]A. C. Ferrari and J. Robertson, Phys. Rev. B **61**, 14095 (2000).
[48]F. Tuinstra and J. L. Koenig, J. Chem. Phys. **53**, 1126 (1970).
[49]S. Piscanec, M. Lazzeri, J. Robertson, A. C. Ferrari, and F. Mauri, Phys. Rev. B **75**, 035427 (2007).
[50]M. Lazzeri, S. Piscanec, F. Mauri, A. C. Ferrari, and J. Robertson, Phys. Rev. B **73**, 155426 (2006).
[51]A. C. Ferrari, J. C. Meyer, V. Scardaci, C. Casiraghi, M. Lazzeri, F. Mauri, S. Piscanec, D. Jiang, K. S. Novoselov, S. Roth, and A. K. Geim, Phys. Rev. Lett. **97**, 187401 (2006).
[52]A. Jorio, A. G. Souza, G. Dresselhaus, M. S. Dresselhaus, A. K. Swan, M. S. Unlu, B. B. Goldberg, M. A. Pimenta, J. H. Hafner, C. M. Lieber, and R. Saito, Phys. Rev. B **65**, 155412 (2002).
[53]F. Bonaccorso, T. Hasan, P. H. Tan, C. Sciascia, G. Privitera, G. Di Marco, P. G. Gucciardi, and A. C. Ferrari, J. Phys. Chem. C **114**, 17267 (2010).
[54]S. M. J. Kelly, Electron. Lett. **28**, 806 (1992).
[55]K. Tamura, E. P. Ippen, and H. A. Haus, IEEE Photonics Technol. Lett. **6**, 1433 (1994).
[56]N. Vukovic, N. G. R. Broderick, M. Petrovich, and G. Brambilla, IEEE Photonics Technol. Lett. **20**, 1264 (2008).
[57]T. A. Birks and Y. W. Li, J. Lightwave Technol. **10**, 432 (1992).